JACS
JOURNAL OF THE AMERICAN CHEMICAL SOCIETY
Article
pubs.acs.org/JACS

Interplay of Ion–Water and Water–Water Interactions within the Hydration Shells of Nitrate and Carbonate Directly Probed with 2D IR Spectroscopy

Joseph A. Fournier,[†] William Carpenter,[†] Luigi De Marco,[†,‡] and Andrei Tokmakoff*[,†]

[†]Department of Chemistry, Institute for Biophysical Dynamics, and James Franck Institute, The University of Chicago, Chicago, Illinois 60637, United States

[‡]Department of Chemistry, Massachusetts Institute of Technology, Cambridge, Massachusetts 02139, United States

Supporting Information

ABSTRACT: The long-range influence of ions in solution on the water hydrogen-bond (H-bond) network remains a topic of vigorous debate. Recent spectroscopic and theoretical studies have, for the most part, reached the consensus that weakly coordinating ions only affect water molecules in the first hydration shell. Here, we apply ultrafast broadband two-dimensional infrared (2D IR) spectroscopy to aqueous nitrate and carbonate in neat H_2O to study the solvation structure and dynamics of ions on opposite ends of the Hofmeister series. By exciting both the water OH stretches and ion stretches and probing the associated cross-peaks between them, we are afforded a comprehensive view into the complex nature of ion hydration. We show in aqueous nitrate that weak ion–water H-bonding leads to water–water interactions in the ion solvation shells dominating the dynamics. In contrast, the carbonate CO stretches show significant mixing with the water OH stretches due to strong ion–water H-bonding such that the water and ion modes are intimately correlated. Further, the excitonic nature of vibrations in neat H_2O, which spans multiple water molecules, is an important factor in describing ion hydration. We attribute these complex dynamics to the likely presence of *intermediate*-range effects influenced by waters beyond the first solvation shell.

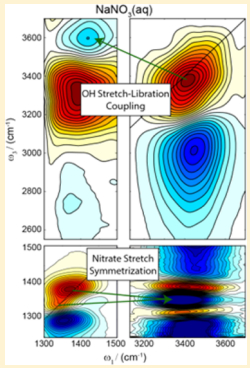

1. INTRODUCTION

The thermodynamic and physical properties of salt solutions derived from the dynamical ion–water interactions and solvation structure are critical for understanding fundamental processes in biological, environmental, and aqueous chemistry. However, despite years of ongoing research, there remains a highly contentious debate over the influence of dissolved ions on the long-range structure of water's hydrogen bond (H-bond) network.[1,2] As a result, our knowledge of how ion–water interactions give rise to bulk properties has remained largely empirical. A more complete, molecular-level description of the structural and dynamical interactions between solutes and water are necessary in order to better understand and model, for example, ion transport across cell membranes and ion-driven processes at the water-soil interface, and for the development of new technologies for desalinization and for removing ions from contaminated water supplies.

The nature of ion–water interactions is often described in terms of the structure "maker" or "breaker" concept[3,4] where certain ions either enhance or disrupt the water H-bond network. This ability to strengthen or weaken the H-bond network can qualitatively account for the wide variability in bulk properties of aqueous solutions such as solubility, viscosity, ion conductivity, surface tension, heat capacity, and enthalpy/entropy of solution.[5,6] These differences generally follow the famous Hofmeister series, originally ordered for the ability of ions to precipitate out proteins in solution: $CO_3^{2-} > SO_4^{2-} > H_2PO_4^- > OH^- > F^- > Cl^- > Br^- > NO_3^- > I^- > ClO_4^- > SCN^-$. Ions on the left side of this series are considered structure makers while those on the right are structure breakers. A point of contention in using the structure maker/breaker model to explain the varying physical and thermodynamical properties of aqueous solutions is whether or not ions alter the H-bond network of "bulk" water far from the ion even in the limit of infinite dilution, or if the influence of the ion is limited to the first hydration shell.

More recently, spectroscopic and theoretical investigations have cast doubt on the long-range effects of ions on the bulk water network. X-ray and neutron diffraction,[7,8] Raman[9] and THz[10] spectroscopy, and molecular dynamics (MD) simulations[9−15] (which have, for the most part, focused on the alkali halides) have concluded that weakly coordinating (structure breaker) ions only influence waters in their first solvation shell, thus leaving the bulk waters essentially unchanged from those in the pure liquid. To the contrary, infrared studies[16,17] on large gas-phase water clusters suggest high-valent ions influence the H-bond network well beyond the first solvation shell. These experiments, of course, do not offer any dynamical insight that might yield important differences between bulk water in salt solutions and in the pure liquid that would not be evident in such structure-based studies.

Received: May 18, 2016
Published: July 12, 2016

ACS Publications © 2016 American Chemical Society

DOI: 10.1021/jacs.6b05122
J. Am. Chem. Soc. 2016, 138, 9634−9645

To this end, ultrafast nonlinear infrared spectroscopies have been used to collect a growing data set of key dynamical metrics such as vibrational lifetimes, anisotropy decays, frequency-frequency correlation functions ($C_{\omega\omega}$), and ion-to-bulk water exchange times.[18−35] Due to the incredibly fast and complex relaxation dynamics occurring on sub-200 fs time scales in neat water,[36−39] most experiments to date have relied on isotopically dilute solutions (~5% HOD in H_2O or D_2O) to both slow vibrational relaxation and to offer a more local picture of the ion−water interaction. Weakly coordinating ions like ClO_4^-, BF_4^-, and SCN^- have received the most attention[18,19,28−32] because these ions split the OH stretch into two distinct peaks, one due to waters in the bulk and one from those bound to the ion. These studies have demonstrated that the ion-bound waters display about 2−3 times slower dynamics than solute-free 5% HOD, with $C_{\omega\omega}$ and anisotropy decays typically in the range of 4−5 ps. The corresponding $C_{\omega\omega}$ and anisotropy decays of the bulk water peaks do not vary considerably from the 5% HOD values[40−44] of 1.7 and 2.6 ps, respectively. These observations, therefore, pointed to the scenario where only the first solvation shell water molecules are affected by the ions.

It is not doubted that the first-shell water molecules are most perturbed by the ion. The point of debate is the long-range influence of an ion on the H-bond network of bulk water. Analysis of the ultrafast IR experiments in the OH stretch region are complicated by signal overlap between the ion solvation shell(s) and bulk water, and the use of such high concentrations (typically >3 M) that the very existence of bulk water is in question.[45] Moreover, strongly coordinating ions that are considered structure makers have yet to be studied comprehensively,[33,34] thus important comparisons between different classes of ions have not yet been made with ultrafast IR spectroscopy. As an example, the FTIR spectra of 2 M $NaNO_3$ and Na_2CO_3 as well as that of neat water, normalized to the peak of each water OH stretch, are displayed in Figure 1. It is evident from the IR spectra that these ions have much different behavior in water. The OH stretch in the nitrate solution is blue-shifted by 15 cm^{-1} compared to pure water indicative of weaker H-bonding between ion and water, whereas the carbonate solution displays a broad tail that extends well below 3000 cm^{-1} similar to what is observed in strongly H-bonded systems such as the aqueous proton or hydroxide.[46,47] Most interesting is the clear splitting of the nominally doubly degenerate asymmetric NO stretch of the nitrate ion resulting in two features centered around 1350 and 1400 cm^{-1}, respectively. This splitting has been interpreted in terms of an asymmetric solvation environment[35,48] which results in ensembles of NO groups that are either more (1350 cm^{-1}) or less (1400 cm^{-1}) strongly H-bonded to their first-shell water molecules. The carbonate CO stretch, on the other hand, appears slightly inhomogeneous and likely has a narrower distribution of frequencies compared to nitrate. MD simulations suggest that the carbonate hydration shell is more ordered with a hydration number of 7−9,[12,49] compared to only 6 in nitrate.[12,50] We note that, although the use of 2 M solutions in this study still calls into the question the presence of bulk water (~14 water molecules per ion in $NaNO_3$ and ~10 per ion in Na_2CO_3), recent MD simulations on 2 M NaBr[11] and 2 M $MgCl_2$[51] demonstrated that water molecules beyond the second solvation shell are present at this concentration.

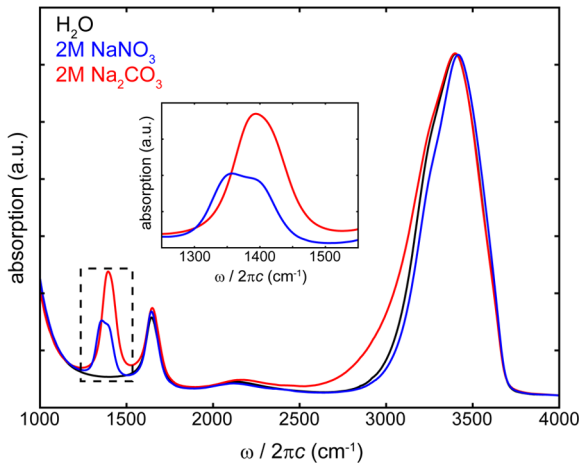

Figure 1. FTIR spectra of H_2O (black), 2 M $NaNO_3$ (blue), and 2 M Na_2CO_3 (red) normalized to their absorption maxima. The asymmetric ion stretch region is shown inset. The nominally doubly degenerate NO stretch in NO_3^- (aq) is split into a partially resolved doublet.

Helbing and co-workers have recently investigated the NO stretch region in aqueous nitrate in neat H_2O using an array of ultrafast spectroscopies.[35] They reported a nitrate stretch lifetime of ~500 fs with an anisotropy decay of 300 fs using two-dimensional infrared (2D IR) spectroscopy. UV-UV and UV-IR studies showed that the reorientation time of the ion was ~2 ps, much longer than the anisotropy decay. It was hypothesized, and supported by MD simulations, that the 300 fs time scale reflects the switching time between the more strongly H-bonded and more weakly H-bonded N−O···H−O interactions, owing to the highly fluctuating nature of the first solvation shell. Moreover, cross-peaks between the two nitrate stretches were uncovered and grew in on the same 300 fs time scale, further supporting this hypothesis. It was also suggested that, on average, there are two more strongly H-bonded ion−water interactions for every one weakly H-bonded interaction.

In this Article, we present a comprehensive study of the aqueous solvation structure and dynamics for two isoelectronic molecular anions on opposite ends of the Hofmeister series, nitrate and carbonate. We extend upon previous spectroscopic studies by also investigating the OH stretches of ion-associated waters and the cross-peaks between anion and water molecules using ultrafast broadband 2D IR spectroscopy. By pumping and probing both the OH stretches and ion stretches, we are able to track short-range ion−water coupling and better investigate longer-range effects manifested through vibrational energy relaxation and coupling to low-frequency intermolecular motions. Moreover, the use of neat H_2O results in ultrafast intra- and intermolecular couplings due to the resonance of the OH stretch oscillators, which are suppressed in studies of isotopically dilute water, and results in qualitatively different ion−water interactions.

2. EXPERIMENTAL METHODS

The 2D IR spectrometer used in this study has been described in detail elsewhere.[52] Briefly, the output of a regenerative amplifier (Coherent Legend USX, 800 nm, 1 kHz, 25 fs) was split into three paths. One path pumps a home-built, two-stage optical parametric amplifier (OPA) which generates 3 μm light used for pumping the water OH stretches.[53] The output can be tuned to cover the 2900−3800 cm^{-1} range. In this study, the pulses were either centered at 3200 or 3400 cm^{-1} with a bandwidth of 350 cm^{-1} fwhm and pulse energies of 4 and 3 μJ, respectively. The pulse width is about 45 fs. A second path

DOI: 10.1021/jacs.6b05122
J. Am. Chem. Soc. 2016, 138, 9634−9645

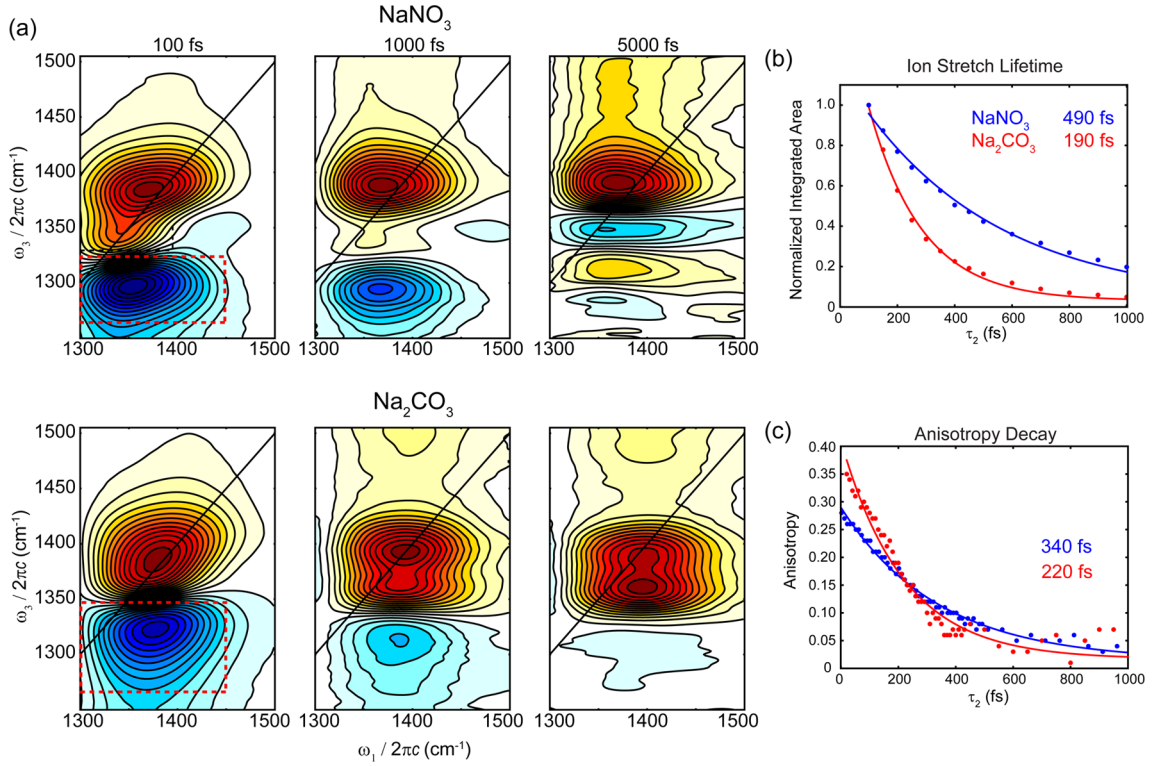

Figure 2. (a) 2D IR spectra of 2 M $NaNO_3$ (top) and Na_2CO_3 (bottom) solutions in H_2O in the ion asymmetric stretch region with 100, 1000, and 5000 fs waiting times. Each spectrum has been individually normalized to the maximum to illustrate the lineshapes. The excited-state absorption decays for the nitrate stretch (blue) and carbonate stretch (red) are shown in panel (b). The anisotropy decays are shown in (c). Integration limits are indicated by the dashed boxes.

pumps a commercial OPA (Light Conversion, TOPAS Prime) generating near-IR signal (1.3−1.5 μm) and idler (1.7−2.0 μm) beams. The signal and idler are combined in $AgGaS_2$ in a home-built difference-frequency generation (DFG) setup, resulting in pump pulses that can be tuned between 4 and 7 μm. In these experiments, the DFG was tuned to generate pulses centered at 1400 cm^{-1} with fwhm of 170 cm^{-1}. The pulse width was measured to be about 90 fs via interferometric autocorrelation with pulse energies of about 4 μJ. Finally, the probe pulse was generated by focusing the first, second, and third harmonic of the third 800 nm leg into a stream of nitrogen. The resulting plasma contains broadband IR spanning <1000 cm^{-1}-4000 cm^{-1} with a pulse width of about 70 fs and pulse energies <1 nJ.[54]

The 3 or 7 μm pump pulses were then split into a pulse pair in a Mach−Zehnder interferometer with variable delay τ_1 using two KBr beamsplitters. One of the interferometer outputs is sent to the sample while the other is monitored with an IR detector to determine the pump spectrum and its phase in order to phase-correct the 2D IR spectra.[55] The fixed arm of the interferometer is chopped at half the repetition rate, 500 Hz. The pump pair and broadband probe are focused into the sample in the pump−probe geometry[56] with a delay τ_2 between the pump and probe pulses, generating a nonlinear polarization that radiates a signal field that is heterodyned with the probe pulse. The signal is dispersed on a 2 × 64 pixel MCT array detector (IR Associates) allowing for the collection of the ω_3 axis in the frequency domain. Half of the probe pulse is directed to the sample while the other half acts as a reference (R) to improve the signal-to-noise ratio. For a given waiting time τ_2, the ω_3 signal on each pixel is monitored as a function of τ_1. The signal S for a given pump pulse i is measured as $I = -\log[(S_i/R_i)(R_{i+1}/S_{i+1})]$ in order to remove the transient absorption signal arising from the moving (unchopped) arm of the interferometer. The Fourier transformation along τ_1 for the resulting signal yields the ω_1 excitation axis. All spectra were collected with magic angle polarization between pump and probe pulses.

For anisotropy measurements, transient absorption spectra were separately collected in the ZZZZ and ZZYY polarization schemes, making sure that the pump power and late-time signals were identical for both polarizations. For the ion-diagonal region, the higher energy ion stretch bleaches near 1400 cm^{-1} were integrated over a 20 cm^{-1} window. For the OH stretch diagonal, the OH bleach was integrated between 3350 and 3450 cm^{-1}. The anisotropy was then calculated as $(I_{par} - I_{perp})/(I_{par} + 2I_{perp})$.

The 2 M samples of sodium nitrate and sodium carbonate (Fischer) were prepared in neat H_2O purified by reverse osmosis to a resistivity of 18 MΩ (Millipore). For each, 1 μL drops were sandwiched between two 1 mm thick CaF_2 windows to achieve an OH stretch peak absorption of <1, resulting in an estimated sample thickness of about 1−2 μm.

3. RESULTS AND DISCUSSION

2D IR spectra for water, nitrate, and carbonate were collected in four regions by pumping in both the OH stretching region ($\lambda \approx 3$ μm) and the ion NO or CO stretching region ($\lambda \approx 7$ μm) and probing the same spectral windows using broadband IR: the ion stretch diagonal, the water OH stretch diagonal, the water-to-ion downhill cross-peak, and the ion-to-water uphill cross-peak. In the following sections we will analyze each of these four quadrants with the aim of arriving at a self-consistent picture of nitrate and carbonate hydration.

3.1. Ion Stretch Diagonal Region. *Results.* The 2D IR spectra in the asymmetric ion stretch region for nitrate and carbonate at 100, 1000, and 5000 fs waiting times are displayed in Figure 2a. The bleaches of the 0 → 1 transitions are colored red and correspond to both ground-state bleaching and stimulated emission from the excited state. The features in blue at lower probe (ω_3) frequencies result from 1 → 2 excited-state absorption induced by the probe after initial excitation to

DOI: 10.1021/jacs.6b05122
J. Am. Chem. Soc. 2016, 138, 9634−9645

the first vibrational state by the pump. These two features are displaced along ω_3 due to the anharmonicity of the potential energy surface. The decays of the excited-state absorption, the most direct reporter of the vibrational lifetime of the ion stretches, are displayed in Figure 2b and were determined by integrating over the areas indicated by the dashed boxes in Figure 2a. The monoexponential decay constant of 490 fs for nitrate is in good agreement with that found by Helbing.[35] The carbonate CO stretch is much shorter lived, with a lifetime decay of 190 fs.

The anisotropy decays for the higher frequency ion stretch bleaches near 1400 cm^{-1} are given in Figure 2c. The 340 fs nitrate anisotropy decay we observe matches that reported by Helbing.[35] As with the ion stretch vibrational lifetime, the carbonate CO stretch anisotropy decays faster than that of nitrate with a time scale of 220 fs.

Discussion. The early time ion stretch bleaches resemble the lineshapes seen in the FTIR spectra (Figure 1) for both species. The nitrate solution displays a clear doubling of the NO stretch, although the lower frequency transition at 1350 cm^{-1} is somewhat masked by overlap with the excited-state absorption. Moreover, the breadth and shift of the bleach off the diagonal in ω_1 indicates the presence of underlying cross-peaks between the two nitrate stretches as was observed by Helbing. The carbonate bleach appears as a single feature with slight inhomogeneous broadening along the diagonal. Surprisingly, the decay of the carbonate stretch is faster than that of the OH stretch in water. The large difference between the nitrate and carbonate ion stretch lifetimes immediately suggests that the carbonate−water interaction is much stronger than that in nitrate such that the CO stretch more rapidly relaxes to the surrounding hydration environment.

The notion of stronger ion−water H-bonding in aqueous carbonate is supported by the ion-stretch anisotropy decays. The 340 fs anisotropy decay in aqueous nitrate is much faster than the physical reorientation time of 2 ps, and is also faster than the 500 fs NO stretch lifetime. We therefore draw conclusions similar to Helbing's:[35] that the nitrate anisotropy decay results from the scrambling of the NO dipole moments induced by fluctuations in the first solvation shell that modulate the H-bonding strength to the three nitrate oxygens. In contrast, the carbonate anisotropy decay is on the order of the CO stretch lifetime. If carbonate is in fact more strongly bound to its first solvation shell, we might expect those hydrating water molecules to be relatively rigid. A tightly bound solvation shell would then result in a longer anisotropy decay time compared to nitrate (ie, a longer time scale for dipole moment scrambling). However, the fact that the anisotropy and stretch lifetime are the same for the CO stretches indicates that these two processes are one in the same. That is, the fast anisotropy decay and vibrational lifetime of the carbonate CO stretches indicates that strong carbonate−water coupling results in the mixing of the ion and water vibrational states such that the initial excitation is delocalized over at least the first hydration shell. This topic will be explored in more detail in later sections, as will the peculiar doublet patterns in the 2D IR spectra observed at the longest waiting times.

3.2. OH Stretch Diagonal Region. *Results.* We next turn to the OH diagonal region, with 2D IR spectra of H_2O, nitrate, and carbonate for waiting times of 100 and 1000 fs displayed in Figure 3. These spectra were collected with the pump frequency centered at 3400 cm^{-1} and a bandwidth of 350 cm^{-1} fwhm. At the earliest waiting times, the OH stretch

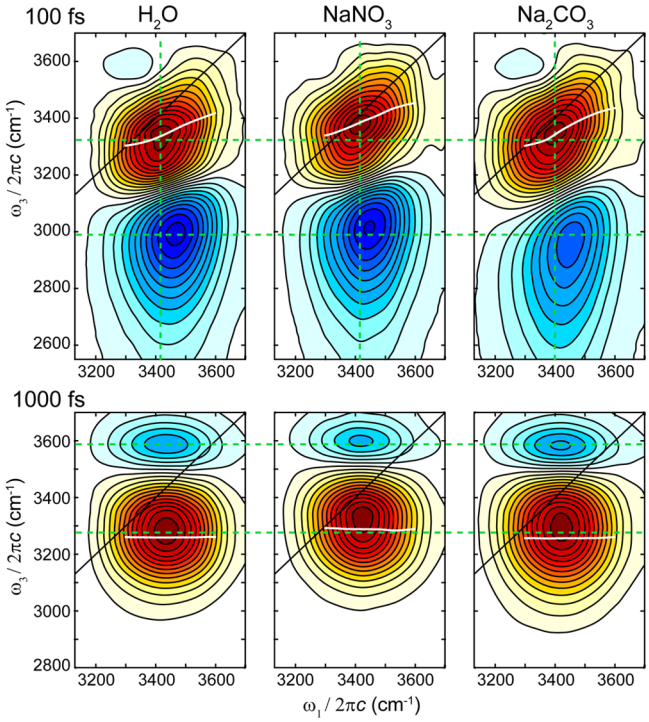

Figure 3. 2D IR spectra of H_2O, 2 M $NaNO_3$, and 2 M Na_2CO_3 in the OH stretch diagonal region taken at 100 fs (top) and 1000 fs (bottom) waiting times, pumping at 3400 cm^{-1}.

bleaches are inhomogeneously broadened along the diagonal with center-line slope values around 0.4 for water and nitrate at 100 fs waiting time. The carbonate OH bleach is more elongated along the diagonal as expected from the broad absorption tail in the FTIR spectrum, resulting in a higher initial value of 0.5. The center-line slope decay provides a direct measure of $C_{\omega\omega}$ and was calculated by fitting the first moment of the bleach in ω_3 along an ω_1 range of 3300−3600 cm^{-1} to a line (indicated by the white lines in Figure 3). The center-line slope of the OH stretch in H_2O was measured to be 170 fs. The decays are marginally slower in nitrate (250 fs) and carbonate (200 fs) solutions.

The large anharmonicities of the OH stretch potential energy surface gives rise to the highly elongated excited-state absorption that peaks near 3000 cm^{-1} but has a tail that extends to our lowest detection frequencies (<1200 cm^{-1}).[36] The decay of this feature is again used to measure the vibrational lifetime of the OH stretch (Figure S1) and is 230 fs in neat H_2O, while it is slightly longer in aqueous nitrate (270 fs) and slightly shorter in aqueous carbonate (190 fs).

The anisotropy decay of the OH stretch in H_2O was measured to be 70 fs, well within the instrument response. The water OH stretch anisotropy decays in nitrate and carbonate solutions are indistinguishable from that of the pure liquid, likely due to the bulk water response (Figure S2).

Discussion. The fast OH stretch lifetime in H_2O has been interpreted in terms of the excitonic nature of the OH stretch vibrations that can span multiple strongly interacting water molecules.[36,57−59] This excitonic behavior is most evident in the fast center-line slope and anisotropy decays, which can be interpreted as a coherent delocalized excitation that quickly loses its frequency and orientational memory due to rapid intermolecular motions. The slowing of relaxation processes relative to pure water is typical of what has previously been

DOI: 10.1021/jacs.6b05122
J. Am. Chem. Soc. 2016, 138, 9634−9645

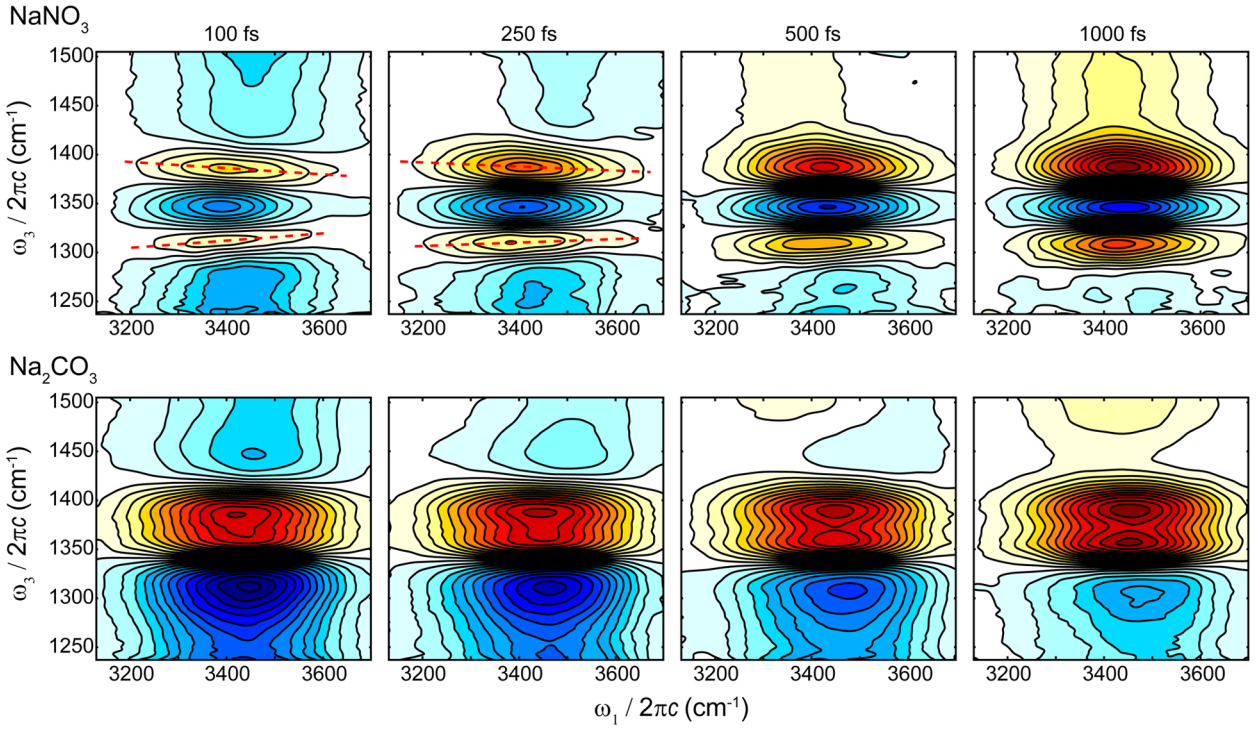

Figure 4. 2 M $NaNO_3$ (top) and Na_2CO_3 (bottom) 2D IR spectra of the ion stretch cross-peaks (pumping at 3400 cm^{-1}) at the indicated waiting times. The spectra for each ion are normalized to the bleach maximum of their respective 1000 fs surface. The weak early time nitrate cross-peak and spectral pattern are accounted for through coupling to low-frequency intermolecular modes which result in the symmetrization of the stretch doublet. In contrast, the strong initial cross-peak in carbonate suggests direct ion stretch−OH stretch mixing.

observed in dilute HOD studies for weakly coordinating ions where the ion acts as a defect to which the water H-bond network must adapt.[19,27] In H_2O, this H-bond weakening in the vicinity of the ion likely results in more localized OH stretch excitation which leads to a slower center-line slope decay. On the other hand, the OH stretch lifetime in carbonate solution is faster than that of water and on the same order as the vibrational lifetime observed for the carbonate CO stretch. This fast relaxation is a result of strong ion−water coupling, perhaps due to Fermi resonance between strongly H-bonded, red-shifted waters coming into resonance with the overtone of the carbonate stretch. This type of CO−HO coupling has been observed in other H-bonded systems.[52] It might be expected that this strong carbonate−water coupling would result in a faster center-line slope decay. However, Auer and Skinner have predicted that both the most strongly and most weakly H-bonded waters in H_2O experience more localized OH stretch character.[57] This has also been suggested experimentally by Mondal and co-workers for both aqueous nitrate and carbonate through line shape analysis of the OH stretch Raman spectra.[60,61] We also cannot neglect the role of the two counter Na^+ ions, whose effects may be imprinted on the observed dynamics.

The rapid vibrational dynamics of the OH stretch in water are also attributed to strong coupling to low-frequency intermolecular modes[38,62−65] and even non-adiabatic couplings[66,67] between these high and low frequency motions due to the strong anharmonicity of the potential energy surface. We will refer to all vibrations of the liquid lower in frequency than the H_2O bend as intermolecular modes and will distinguish between librations (>300 cm^{-1}) and H-bond stretches and distortions (<300 cm^{-1}) where needed. It is known that H-bond vibrations highly influence the frequency of the OH stretch as water molecules fluctuate closer or farther away from their H-bonding neighbors.[68,69] This can result in allowed curve-crossings between the OH stretch and the bend overtone near 3200 cm^{-1}, as recently described by Hamm and Stock.[70] Therefore, it has been proposed that the OH stretch can quickly dissipate into bend motions and intermolecular modes.

The fast dissipation of vibrational energy into intermolecular modes is often used to describe the long-time spectra in Figure 3. As these modes become more populated, fluctuations increase in the liquid resulting in the overall weakening of the H-bond network that results in an OH stretch that is blue-shifted and less intense, thus explaining the appearance of the new excited-state absorption feature at 3600 cm^{-1}. This late-time behavior is referred to in the literature as the "hot ground state" because its spectrum in ω_3 matches what is seen in a ∼10 K thermal difference FTIR spectrum (Figure S3). However, it is emphasized that the hot ground state does not represent an equilibrium state. This is evident from the 100 fs water and carbonate spectra where the hot ground state signal is already growing in even on the quickest time scales of the motions in the liquid. This observation indicates that there are instantaneous changes to the OH stretch manifold following stretch excitation, and evidence presented later suggests it is indeed a result of direct coupling to intermolecular modes. The hot ground state signal grows in on a 680 fs time scale in the pure liquid. As with the center-line slope decay, this value is slightly slower in nitrate (770 fs) and carbonate (700 fs).

3.3. Water-to-Ion Cross-Peak Region. *Results.* The water-to-ion cross-peaks collected at several waiting times after OH stretch excitation at 3400 cm^{-1} are displayed in Figure 4 and are normalized to the respective 1000 fs surfaces to illustrate their change in intensity with waiting time. Spectra

DOI: 10.1021/jacs.6b05122
J. Am. Chem. Soc. 2016, 138, 9634−9645

collected with the pump frequency centered at 3200 cm^{-1} are given in the Supporting Information. The corresponding amplitudes of the bleaches as a function of waiting time are presented in Figure 5 for pumping at 3200 cm^{-1} (red traces)

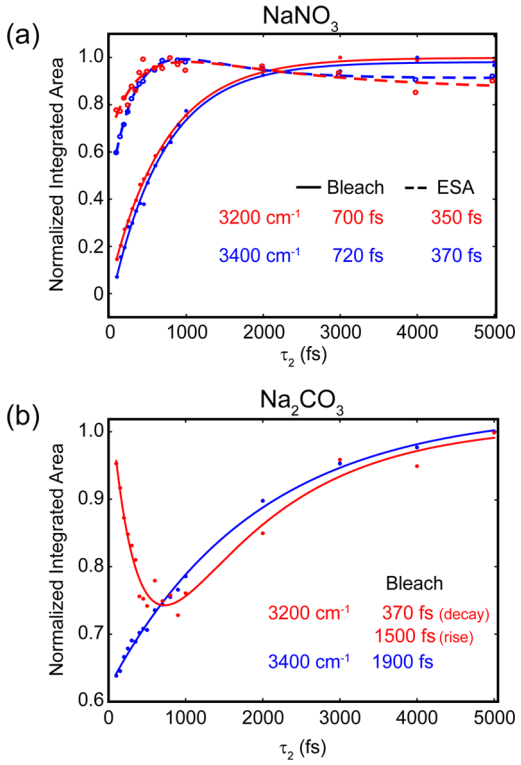

Figure 5. Water-to-ion cross-peaks dynamics when pumping at 3200 cm^{-1} (red) and 3400 cm^{-1} (blue) for (a) NO_3^-(aq) and (b) CO_3^{2-}(aq). The nitrate bleach and excited-state absorption (ESA) dynamics are independent of pump frequency. For carbonate, the bleach dynamics are quite different, with the bleach intensity starting at a maximum when pumping at 3200 cm^{-1}. This indicates direct stretch−stretch mixing with the first-shell water molecules.

and 3400 cm^{-1} (blue traces). For aqueous nitrate, the cross-peak region displays two pairs of bleaches and excited-state absorptions. At short waiting times, both bleaches are very weak, with extrapolated intensities to τ_2 = 0 fs yielding essentially zero signal (Figure 5a). These bleaches grow with τ_2 on 700 fs (ω_3 = 1310 cm^{-1}) and 500 fs (ω_3 = 1380 cm^{-1}) time scales. The low-frequency excited-state absorption near 1250 cm^{-1} decays within 500 fs and is consistent with a 1 + 1 combination band for which cross-peak excited-state absorptions are most commonly derived. The high-frequency excited-state absorption (ω_3 = 1350 cm^{-1}), however, actually gains intensity at early times before plateauing. Importantly, the dynamics of these features do not depend on pump frequency, as illustrated in Figure 5a. We also note the anticorrelated tilts of the two cross-peak bleaches when pumping at 3400 cm^{-1}. These tilts decay on sub-170 fs time scales (Figure S4).

In contrast to nitrate, aqueous carbonate has a strong water-to-ion cross-peak at early waiting time, which grows on a slow 1900 fs time scale. The integrated bleach intensity extrapolated to τ_2= 0 fs begins at 0.6 relative to its value at τ_2 = 5000 fs when pumped at 3400 cm^{-1}. Additionally, the bleach line shape evolves from a single peak into a clear doublet structure at longer waiting times. Aqueous carbonate also shows a striking pump-frequency dependence. When the pump frequency is tuned to the strongly H-bonded waters at 3200 cm^{-1}, the strong cross-peak actually decays at first with a 370 fs time constant before growing at longer waiting times (Figure 5b). The single excited-state absorption at 1325 cm^{-1} decays on 460 and 550 fs time scales when pumping at 3200 and 3400 cm^{-1}, respectively.

Discussion. While the water-to-nitrate cross-peak lineshapes could be interpreted as the first hydration shell directly coupling to the two NO stretches, we note that the cross-peak region looks nearly identical to the long-time nitrate stretch diagonal region (Figure 2a, 5000 fs). Moreover, the doublet pattern in ω_3 match what is observed in a FTIR thermal difference spectrum (Figure S3). These observations indicate that, as a result of the highly mixed water OH stretch−intermolecular mode manifold, OH excitation induces increased water H-bond fluctuations around the ion resulting in the rapid symmetrization of the nitrate stretches. Thus, the growth of the two bleaches, which again initially have zero intensity, results from the narrowing of the nitrate stretch distribution and gives rise to the growing excited-state absorption feature between the bleaches.

The anti-correlated tilts of the two bleaches provide direct evidence for the water-induced symmetry breaking of the ion stretches. As the H-bonding strength between the first-shell water molecules and the ion increases, the OH absorption frequency ω_1 is reduced, and one of the nitrate resonance structures is further stabilized, resulting in a larger splitting between the two nitrate bleaches. This memory of the initial solvent configuration is short-lived, with the decay time consistent with the period of a H-bond vibration. Taken together, the water-to-nitrate cross-peak lineshapes and dynamics can be explained through the interaction between nitrate and OH stretching vibrations mediated primarily through their H-bonding rather than direct OH-stretch to NO-stretch coupling.

In the case of aqueous carbonate, the fact that a strong cross-peak bleach is present at 0 fs means that the OH stretches and carbonate stretches are indeed strongly anharmonically mixed such that excitation of one manifold necessarily causes excitation of the other. In other words, the carbonate stretches contain significant OH character and vice versa. The signal at early times, therefore, is dominated by this strong, direct ion stretch−OH stretch mixing, rather than the weaker intermolecular mode-mediated interaction in aqueous nitrate that gives rise to the doubling structure at later times.

To help clarify the nature of the ion−water interactions, we also pumped the low-frequency portion of the OH absorption spectra by centering our pump frequency at 3200 cm^{-1}. Shifting the pump frequency gives us access to the red-shifted tail in carbonate arising from strongly H-bonded waters and allows us to examine the effects of pumping non-solvation waters in the nitrate solution. In aqueous nitrate, the 3200 cm^{-1} cross-peak region displays essentially identical dynamics compared to pumping at 3400 cm^{-1}. Since these strongly red-shifted OH oscillators at 3200 cm^{-1} in aqueous nitrate are not expected to be ion-bound, the nearly identical spectra and dynamics confirm the picture that water−water interactions between OH stretches of the first and second solvation shells are stronger than their interactions with nitrate, and that there is little direct mixing of water OH and nitrate NO vibrations.

In aqueous carbonate, with the pump frequency now centered at 3200 cm^{-1} the bleach starts at a maximum at τ_2 = 0 fs and initially decays before growing at later times due to

DOI: 10.1021/jacs.6b05122
J. Am. Chem. Soc. 2016, 138, 9634−9645

the expected intermolecular mode coupling, vibrational relaxation, and hot ground state effects. This is clear evidence of the direct mixing of the carbonate stretches with OH stretches within the first solvation shell when pumping at 3200 cm^{-1}, with the initial 370 fs decay time interpreted as the lifetime of this mixed state.

These observations for aqueous nitrate and carbonate raise the important question of whether we can actually distinguish between first- and outer-shell excitation and response. The large pump-frequency dependence seen in the carbonate cross-peak dynamics would indicate that we can indeed separate the responses in aqueous carbonate. The fact that the 3400 cm^{-1} water-to-carbonate cross-peaks in Figure 4 display significant stretch−stretch mixing contributions yet drastically different dynamics compared to the 3200 cm^{-1} cross-peak indicates that the direct ion−water mixing extends beyond the first shell. This observation is in agreement with the Raman line shape analysis performed by Mondal and co-workers, which indicated the presence of strongly H-bonded outer-shell water molecules in aqueous Na_2CO_3.[61]

In nitrate, since the lineshapes and dynamics are identical, the separation of responses is not possible. It would seem, therefore, that the excitonic and intermolecular mode couplings are blurring the distinction between first- and outer-shell water molecules in aqueous nitrate. Indeed, it has been predicted that the OH stretch exciton can span as many as six molecules in the pure liquid.[57] The addition of strong intermolecular mode coupling means that, upon OH stretch excitation, there is a very complex set of coupled high- and low-frequency motion that spans several water molecules. Therefore, it seems likely that the excitation of the first shell will induce stretch and/or intermolecular motion within the second shell and vice versa. We again emphasize that such behavior will not be observed in dilute HOD where the effects of these couplings are suppressed. As a consequence, the real question regarding longer-range effects is how water−water interactions that depend on excitonic and intermolecular motions are influenced in outer hydration shells by the presence of a solute.

3.4. Ion-to-Water Cross-Peak Region. *Results.* The ion-to-water OH stretch cross-peaks generated by pumping at 7 μm for neat H_2O, NO_3^-(aq), and CO_3^{2-}(aq) at 100 fs are shown in Figure 6. The long waiting-time spectra are essentially identical to the 1000 fs OH stretch hot ground state signal recorded at 3 μm in Figure 3 and thus are a result of the same relaxation mechanism (Figure S5). What is unexpected, however, is the immediate appearance of this apparent hot ground state signal at the earliest waiting times. (The signal observed for $\omega_1 < 1350$ cm^{-1} is from the non-resonant response of the CaF_2 windows due to slight pulse overlap and/or residual chirp of the broadband probe, which rapidly decays and does not affect the analysis given below.)

The growth dynamics of the excited-state absorption signals near $\omega_3 = 3600$ cm^{-1} with τ_2 for the three species are given in Figure 7. Interestingly, the intensity of this feature in pure water remains nearly constant over the entire 5000 fs range. The corresponding feature in aqueous carbonate, on the other hand, displays a well-defined exponential growth of 850 fs. Aqueous nitrate once again displays significantly different behavior. At early times, the excited-state absorption signal is noisy and relatively constant like water, but does increase at later times on a much slower 1800 fs time scale.

The growth of the ion-to-water OH cross-peak bleach for each species is plotted in Figure 8. Since the spectral responses

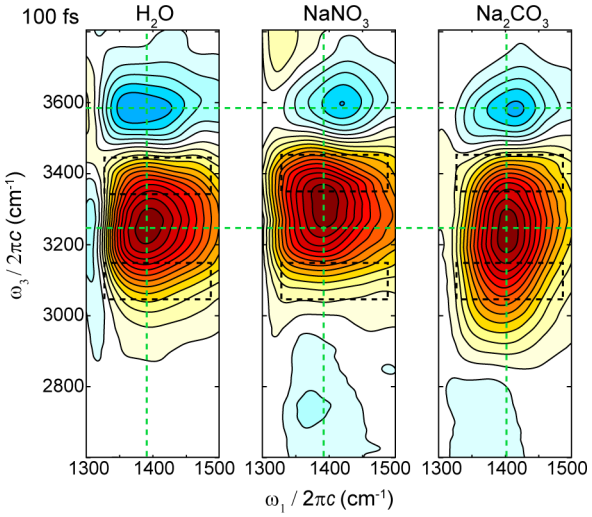

Figure 6. OH stretch cross-peak taken by pumping at 7 μm for H_2O, 2 M $NaNO_3$, and 2 M Na_2CO_3 at 100 fs. The immediate appearance of hot ground state signal at 100 fs for water demonstrates that this pattern results from strong OH stretch−intermolecular mode coupling.

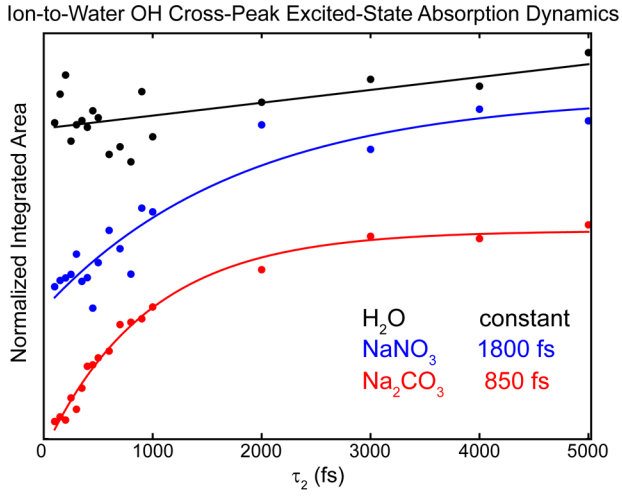

Figure 7. Ion-to-water OH stretch cross-peak dynamics of the excited-state absorption feature at 3600 cm^{-1}. The fits have been displaced along the *y*-axis for better comparison.

of first- and outer-shell waters overlap, we integrate the bleach signals over a low-frequency (3100 cm^{-1}) and a high-frequency (3400 cm^{-1}) region to try to better understand the differences in dynamics between weakly and strongly H-bonded water molecules. The integration areas are indicated in Figure 6. For water and aqueous carbonate, the low-frequency integration yields a fast 200 fs growth, while integrating over the high-frequency section results in a slower 500 fs time scale. The OH cross-peak bleach growth in aqueous nitrate, however, is much slower over both integration regions with time constants of 630 and 900 fs for the red and blue portions of the bleach, respectively.

Discussion. For the two ions, the OH stretch cross-peak bleach lineshapes in ω_3 closely resemble the frequency distributions on the low-frequency wing of the OH stretch FTIR spectra in those solutions (Figure S6). The low-frequency excited-state absorption near $\omega_3 = 2700$ cm^{-1} observed in the ion solutions likely correspond to either

DOI: 10.1021/jacs.6b05122
J. Am. Chem. Soc. 2016, 138, 9634−9645

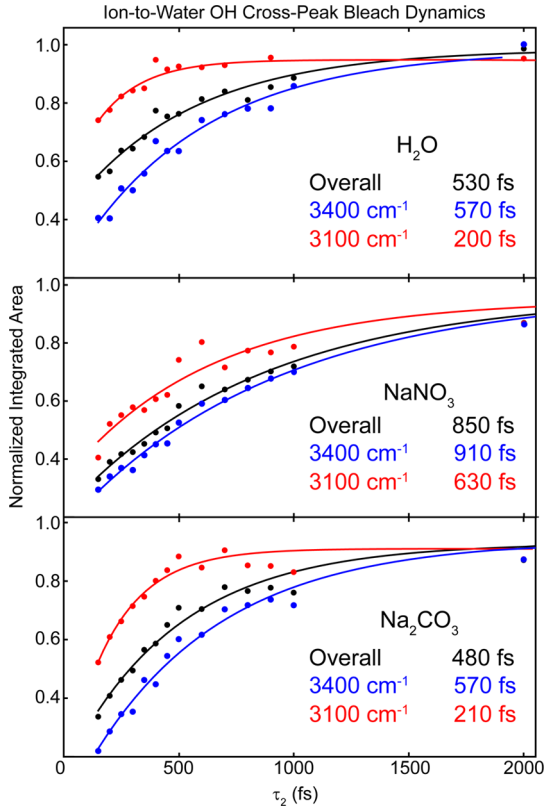

Figure 8. Ion-to-water cross-peak bleach growth for H_2O (top), 2 M $NaNO_3$ (middle), and 2 M Na_2CO_3 (bottom). The overall bleach growth determined by integrating over the entire feature is given in black. Growth dynamics for a low-frequency section (3100 cm^{-1}) is in red while the growth for a high-frequency (3400 cm^{-1}) section is given in blue. The integration limits are given by the boxes in Figure 6.

ion−water combination bands or intramolecular ion overtones/combination bands, where the latter have been observed in resonance Raman.[71] This feature decays within 200 fs in aqueous nitrate, but interestingly grows with waiting time in aqueous carbonate. Moreover, the most red-shifted section of the OH bleach in aqueous carbonate below 3000 cm^{-1} actually decays with waiting time (Figures S5, S6, S14). These observations suggest that the most strongly H-bonded waters in the first solvation shell of carbonate not only become repopulated but become even stronger at longer times. We have not yet considered the consequences of the $CO_3^{2-} + H_2O \rightarrow HCO_3^- + OH^-$ acid−base reaction. A 2 M carbonate solution will contain about 0.4 mM each of hydroxide and bicarbonate. These concentrations are well below the sensitivity of our experiments for direct detection, although the observed dynamics could certainly be influenced. Since the acid−base reaction is endothermic, it is plausible that the dissipation of vibrational energy drives the reaction toward the product side of the potential energy surface such that the system could now be accessing higher-energy portions of the reactive surface. Thus, stronger hydroxide-like waters in the first solvation shell might now be contributing to the signal at late times. Further studies of this process are warranted and could offer new insight into the fundamentals of acid−base reactions and equilibria.

The appearance of the high-frequency excited-state absorption at ω_3 = 3600 cm^{-1}, reminiscent of the hot ground state spectra discussed earlier, in the ion-to-water cross-peak region is quite telling about the OH stretch−intermolecular mode coupling in aqueous systems. The fact that a hot ground state-like signal appears in pure water confirms that strong mixing between water librations and the OH stretch is the key contributor to the hot ground state signal.[62,63,72] We also cannot rule out the possibility that the low-frequency H-bond vibrations are being excited directly through a Raman-like process. In either case, our interpretations are unaffected. Since this feature appears in neat H_2O at even 100 fs and remains nearly constant over the entire 5000 fs waiting time, it is evident that this excited-state absorption signal is the direct manifestation of the coupling between the low-frequency librational and high-frequency OH stretching coordinates, although the exact mechanism giving rise the hot ground state signal is still not well understood.

In the nitrate solution, the noisy early time ω_3 = 3600 cm^{-1} excited-state absorption signal can be assigned to water libration excitation with little contribution from the ion itself since the nitrate and water stretches interact very weakly and do not result in stretch−stretch mixing. Interestingly, the slow 1800 fs growth of this feature in aqueous nitrate matches the time for ion reorientation and water H-bond rearrangement. This is further evidence that the nitrate−water H-bond is so weak that vibrational energy in the ion does not fully dissipate to the solvent intermolecular modes until overall reorganization of the ion solvation structure occurs. For aqueous carbonate, the well-defined growth of the 3600 cm^{-1} feature can be attributed to the time it takes for all the initially mixed carbonate−water vibrational energy to decay into the intermolecular modes.

The ion-to-water cross-peak bleach signal encodes several processes: direct ion stretch−OH stretch coupling, water libration-stretch coupling, and the weakening of the H-bond network through vibrational energy relaxation. The latter process is manifested through both a blue shift of the OH stretch and the loss of OH stretch oscillator strength. In fact, it is clear from FTIR 10 K difference spectra (Figure S7) that the loss of OH intensity is the dominant manifestation of H-bond weakening. Thus, the OH bleach growth should provide the most sensitive probe of changes in the H-bond network. The fast 200 fs growth of the low-frequency 3100 cm^{-1} section of the bleach in H_2O shows that the most strongly H-bonded waters bleach first followed by the more weakly bound waters. Since high-frequency librations near 7 μm are likely associated with more strongly H-bonded water molecules, we interpret the fast low-frequency OH bleach growth in H_2O to direct stretch−libration coupling within strongly H-bonded molecules. The slower 500 fs growth of the high-frequency 3400 cm^{-1} portion of the bleach is an indication of the time scale for vibrational relaxation to lower-frequency intermolecular modes.

Note that the bleach dynamics in aqueous carbonate are essentially identical to those in pure water. This suggests that the strength of the water−water interactions in the carbonate solution is similar to that in the pure liquid. Further, the immediate bleaching of the low-frequency tail of the OH stretch in aqueous carbonate again points to direct ion−water coupling.

The OH stretch cross-peak bleach in aqueous nitrate, however, grows with much slower time scales. If the most strongly bound, red-shifted waters in the nitrate solution behaved just like bulk water and were not influenced by the ion, we would expect similar OH bleach growth dynamics as those observed for H_2O. This behavior is not observed, suggesting

DOI: 10.1021/jacs.6b05122
J. Am. Chem. Soc. 2016, 138, 9634−9645

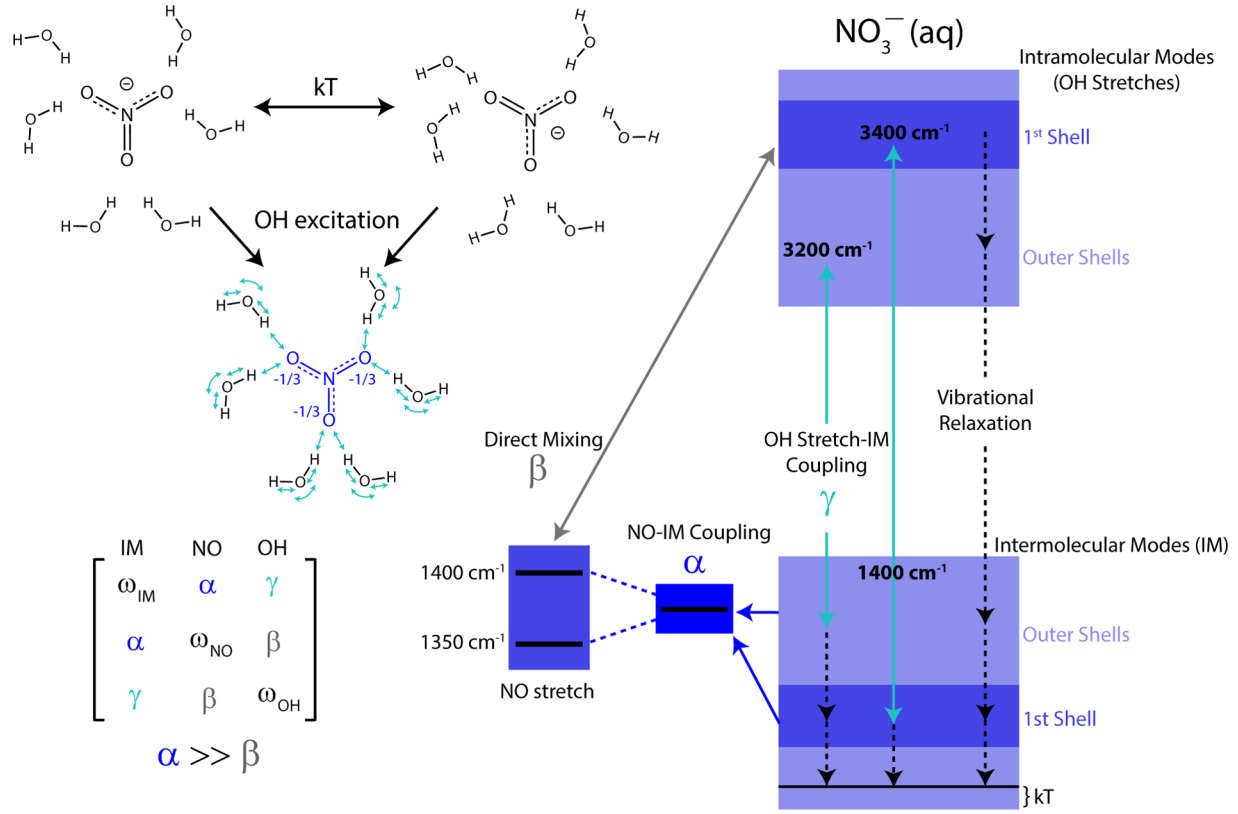

Figure 9. Energy-level diagram of the OH stretching, intermolecular mode (IM), and NO stretching manifolds in aqueous nitrate. The observed spectra and dynamics can be attributed to the strong OH stretch−IM coupling (γ). The highly fluctuating hydration shell causes the observed splitting of the nitrate stretches. Upon OH stretch excitation, the coupling to low-frequency IM within both the first and outer solvation shells in nitrate results in the immediate symmetrization of the nitrate stretches (α).

that the most red-shifted waters in aqueous nitrate are associated with less strongly H-bonded, lower-frequency librational motions. Thus, more time is needed to bleach the OH stretch in aqueous nitrate because there is a lower population of water molecules which have high-frequency 7 μm librations. Energy in the excited nitrate stretch must dissipate to low-frequency modes in order to grow the bleach, which happens on a slow time scale. The observed slower coupling and energy transfer dynamics indicate the presence of weaker water−water H-bond interactions between nitrate's outer-shell water molecules compared to those in the pure liquid.

4. SUMMARY AND CONCLUSIONS

We summarize our findings qualitatively in the energy-level diagrams in Figures 9 and 10 which display the relative frequencies of the water OH stretch and libration manifolds and the nitrate and carbonate asymmetric ion stretches, respectively. In general, a strengthening of the H-bonding interactions of water with its solute lowers the OH stretch frequency and raises the frequency of the associated librational and H-bond intermolecular motions. In pure water and both aqueous solutions, strong coupling between the OH stretch and intermolecular mode manifolds results in an immediate response from all modes upon excitation of the stretches, bends, or intermolecular modes. This mixing results in an immediate appearance of the hot ground state signal at the earliest waiting times regardless of pump frequency. For nitrate (Figure 9), the highly fluctuating solvation shell resulting from weak ion−water H-bonding causes a large distribution of NO stretch frequencies which act to stabilize certain resonance structures, thus leading to the observed splitting in the FTIR spectrum. Upon OH stretch excitation, the immediate OH stretch−intermolecular mode coupling (γ) results in the rapid symmetrization of the nitrate asymmetric stretch distribution due to the increase of low-frequency motion around the ion (α). This symmetrization appears to occur whether exciting the first- or outer-shell water molecules due to the excitonic and intermolecular nature of OH stretch excitation. We do not observe evidence for direct nitrate stretch−OH stretch mixing (β).

In carbonate (Figure 10), the dominant contributor is the direct mixing (δ) between carbonate and water modes in both the first and (at the least) second solvation shells. Similar OH stretch−intermolecular mode coupling as well as vibrational energy relaxation also results in the narrowing of the CO line shape at longer waiting times (ε). Critically, there is a key balance being struck between ion−water and water−water H-bonding interactions in these two systems.

Alternatively, we can describe the ion−water interactions in terms of an eigenstate representation that includes the ion stretch, the water OH stretch, and water intermolecular modes. The off-diagonal matrix elements between ion stretch and OH stretch, δ, are relatively large in aqueous carbonate when compared with water OH−OH interactions (γ), but are small in aqueous nitrate. In nitrate, the off-diagonal terms between ion-intermolecular mode (α) and OH stretch−intermolecular mode (γ) are the main contributors to the observed nitrate−water interaction. The differences in these contributions can be related to the strength of the ion−water H-bond. The strong carbonate−water H-bond results in a more rigid solvation shell

DOI: 10.1021/jacs.6b05122
J. Am. Chem. Soc. 2016, 138, 9634−9645

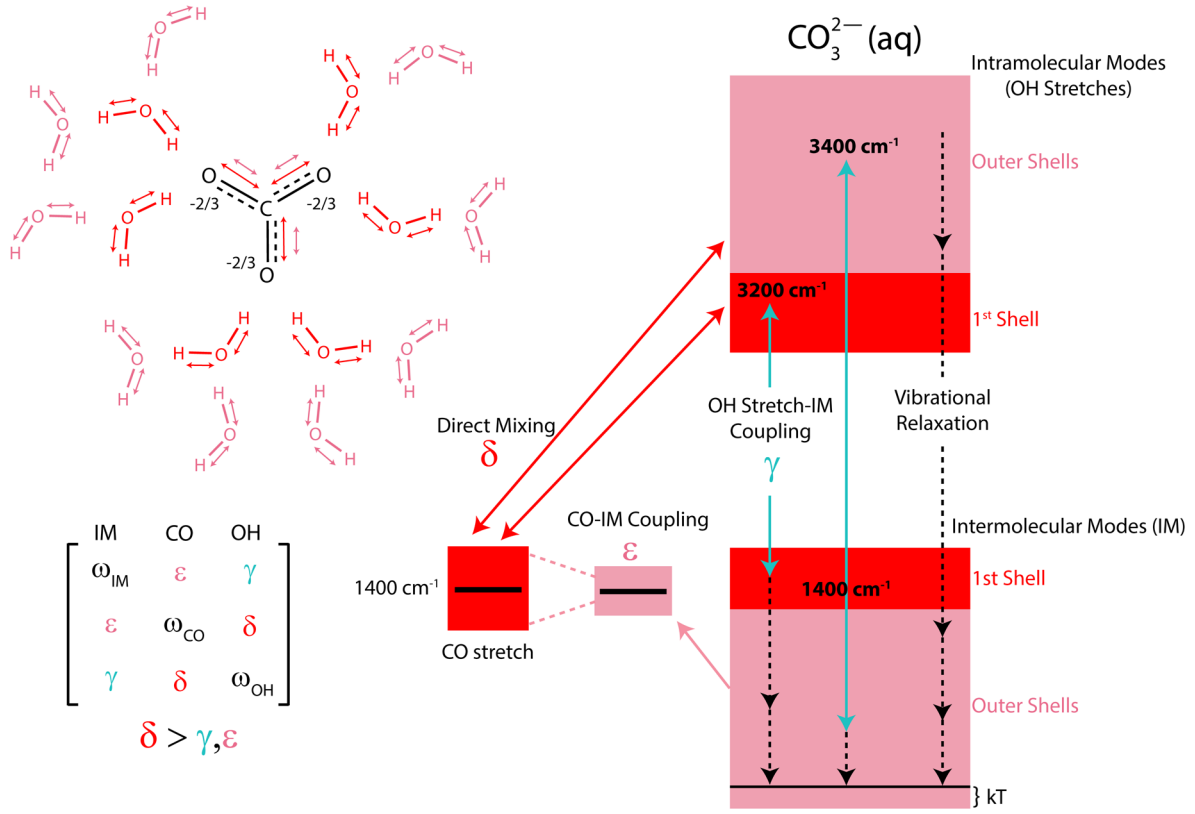

Figure 10. Energy-level diagram of the OH stretching, intermolecular mode (IM), and CO stretching manifolds in aqueous carbonate. The spectra and dynamics are dominated by the strong, direct mixing (δ) between the ion and water modes which extend to at least the second solvation shell. OH stretch−IM coupling (γ) also results in the narrowing of the CO stretch distribution at longer waiting times (ε).

which suppresses intermolecular motion and drives highly mixed ion−water stretching that possibly spans the entire solvated complex, as has been suggested in aqueous hydroxide.[73] In contrast, the much weaker nitrate−water H-bond causes a fluctuating solvation shell such that both the ion stretch and OH stretch frequencies are highly sensitive to the intermolecular separation. This separation is, of course, driven by low-frequency motion which explains why the nitrate−water interaction is dominated by coupling to intermolecular modes.

Although the 2 M solutions used in this study may not be an accurate representation of solvation water in the dilute limit, our results provide evidence that one can use time-resolved IR spectroscopy to study the effects of the ions on the second solvation shell. Even though nitrate does not affect the frequency distribution of water molecules beyond the first shell, we can consider the *dynamical* effects to the H-bond network encoded in metrics like hot ground state growth and vibrational energy relaxation which are a result of the strong OH stretch−intermolecular mode coupling. Since they are only available in *neat* H_2O where the excitonic nature of the OH stretch is critical, until now these metrics have not been carefully considered as a source of information on aqueous solvation shells.

Much of the disparity between previous studies and this one can be attributed to the use of dilute HOD in the former, where the effects of the highly complex couplings in neat H_2O are suppressed. Given the wide range of contemporary experimental and theoretical studies that point to small outer-shell effects, it seems unlikely that a weakly H-bonding ion like nitrate will cause long-range changes in the overall H-bond network in the dilute limit. However, the excitonic nature of the OH stretch and the strong coupling between high and low-frequency modes in neat H_2O means that we should consider the *intermediate*-range effects on the H-bond network which arise from these complex motions spanning multiple water molecules.

Since water's excitonic vibrations are difficult to address conceptually and theoretically, our conclusions at this point remain largely qualitative. However, it is our hope that these experiments spur interest in the theory of excitonic vibrations in naturally occurring H_2O interacting with ions and other solutes. We believe that the newly characterized dynamical metrics reported here and continued experimental developments to directly probe the ion−water interactions will help guide new theoretical models to more accurately simulate and predict the behavior and properties of aqueous salt solutions and neat water itself.

■ ASSOCIATED CONTENT

Supporting Information

The Supporting Information is available free of charge on the ACS Publications website at DOI: 10.1021/jacs.6b05122.

Figures S1 and S2, OH stretch diagonal region dynamics pumping at 3400 cm^{-1} and anisotropy decay for all three species; Figure S3, comparison of 10 K FTIR thermal difference spectra with 2D IR ω_3 projections; Figure S4, nitrate NO cross-peak bleach center-line slope decays; Figure S5, comparison of ion-to-water late-time OH cross-peaks to late-time OH diagonal hot ground-state spectra; Figure S6, comparison of the ion-to-water OH cross-peak ω_3-projections and several dynamical metrics;

DOI: 10.1021/jacs.6b05122
J. Am. Chem. Soc. 2016, 138, 9634−9645

Figure S7, FTIR spectra in the OH stretch region taken at 23 and 33 °C; Figures S8−S11, overview 2D IR spectra at 100 fs waiting time for each of the four quadrants investigated; Figure S12, comparison of water-to-nitrate cross-peak region for pumping at 3200 vs 3400 cm^{-1}; Figure S13, comparison of water-to-carbonate cross-peak region for pumping at 3200 vs 3400 cm^{-1}; Figure S14, overview of ion-to-water OH cross-peaks at several waiting times (PDF)

AUTHOR INFORMATION

Corresponding Author

*tokmakoff@uchicago.edu

Notes

The authors declare no competing financial interest.

ACKNOWLEDGMENTS

This work was supported by the U.S. Department of Energy under grant DE-SC0014305.

REFERENCES

(1) Tobias, D. J.; Hemminger, J. C. *Science* **2008**, *319*, 1197−1198.
(2) Chen, Y.; Okur, H. I.; Gomopoulos, N.; Macias-Romero, C.; Cremer, P. S.; Petersen, P. B.; Tocci, G.; Wilkins, D. M.; Liang, C.; Ceriotti, M.; Roke, S. *Sci. Adv.* **2016**, *2*, e1501891.
(3) Marcus, Y. *Chem. Rev.* **2009**, *109*, 1346−1370.
(4) Ohtaki, H.; Radnai, T. *Chem. Rev.* **1993**, *93*, 1157−1204.
(5) Marcus, Y. *J. Chem. Soc., Faraday Trans. 1* **1986**, *82*, 233−242.
(6) Marcus, Y. *J. Chem. Soc., Faraday Trans. 1* **1987**, *83*, 339−349.
(7) Mancinelli, R.; Botti, A.; Bruni, F.; Ricci, M. A.; Soper, A. K. *J. Phys. Chem. B* **2007**, *111*, 13570−13577.
(8) Burke, C. A. E.; Adya, A. K.; Neilson, G. W. A. *J. Phys.: Condens. Matter* **1991**, *3*, 837−850.
(9) Smith, J. D.; Saykally, R. J.; Geissler, P. L. *J. Am. Chem. Soc.* **2007**, *129*, 13847−13856.
(10) Funkner, S.; Niehues, G.; Schmidt, D. A.; Heyden, M.; Schwaab, G.; Callahan, K. M.; Tobias, D. J.; Havenith, M. *J. Am. Chem. Soc.* **2012**, *134*, 1030−1035.
(11) Lin, Y. S.; Auer, B. M.; Skinner, J. L. *J. Chem. Phys.* **2009**, *131*, 13.
(12) Vchirawongkwin, V.; Kritayakornupong, C.; Tongraar, A.; Rode, B. M. *J. Phys. Chem. B* **2011**, *115*, 12527−12536.
(13) Verde, A. V.; Lipowsky, R. *J. Phys. Chem. B* **2013**, *117*, 10556−10566.
(14) Stirnemann, G.; Wernersson, E.; Jungwirth, P.; Laage, D. *J. Am. Chem. Soc.* **2013**, *135*, 11824−11831.
(15) Nigro, B.; Re, S.; Laage, D.; Rey, R.; Hynes, J. T. *J. Phys. Chem. A* **2006**, *110*, 11237−11243.
(16) O'Brien, J. T.; Williams, E. R. *J. Am. Chem. Soc.* **2012**, *134*, 10228−10236.
(17) DiTucci, M. J.; Heiles, S.; Williams, E. R. *J. Am. Chem. Soc.* **2015**, *137*, 1650−1657.
(18) Moilanen, D. E.; Wong, D.; Rosenfeld, D. E.; Fenn, E. E.; Fayer, M. D. *Proc. Natl. Acad. Sci. U. S. A.* **2009**, *106*, 375−380.
(19) Fayer, M. D.; Moilanen, D. E.; Wong, D.; Rosenfeld, D. E.; Fenn, E. E.; Park, S. *Acc. Chem. Res.* **2009**, *42*, 1210−1219.
(20) Giammanco, C. H.; Wong, D. B.; Fayer, M. D. *J. Phys. Chem. B* **2012**, *116*, 13781−13792.
(21) Yuan, R. F.; Yan, C.; Tamimi, A.; Fayer, M. D. *J. Phys. Chem. B* **2015**, *119*, 13407−13415.
(22) Kuo, C. H.; Vorobyev, D. Y.; Chen, J. X.; Hochstrasser, R. M. *J. Phys. Chem. B* **2007**, *111*, 14028−14033.
(23) Vorobyev, D. Y.; Kuo, C. H.; Chen, J. X.; Kuroda, D. G.; Scott, J. N.; Vanderkooi, J. M.; Hochstrasser, R. M. *J. Phys. Chem. B* **2009**, *113*, 15382−15391.
(24) Vorobyev, D. Y.; Kuo, C. H.; Kuroda, D. G.; Scott, J. N.; Vanderkooi, J. M.; Hochstrasser, R. M. *J. Phys. Chem. B* **2010**, *114*, 2944−2953.
(25) Omta, A. W.; Kropman, M. F.; Woutersen, S.; Bakker, H. J. *Science* **2003**, *301*, 347−349.
(26) Timmer, R. L. A.; Bakker, H. J. *J. Phys. Chem. A* **2009**, *113*, 6104−6110.
(27) Tielrooij, K. J.; Garcia-Araez, N.; Bonn, M.; Bakker, H. J. *Science* **2010**, *328*, 1006−1009.
(28) Park, S.; Odelius, M.; Gaffney, K. J. *J. Phys. Chem. B* **2009**, *113*, 7825−7835.
(29) Gaffney, K. J.; Ji, M. B.; Odelius, M.; Park, S.; Sun, Z. *Chem. Phys. Lett.* **2011**, *504*, 1−6.
(30) Ji, M.; Gaffney, K. J. *J. Chem. Phys.* **2011**, *134*, 044516.
(31) Bian, H. T.; Wen, X. W.; Li, J. B.; Chen, H. L.; Han, S. Z.; Sun, X. Q.; Song, J. A.; Zhuang, W.; Zheng, J. R. *Proc. Natl. Acad. Sci. U. S. A.* **2011**, *108*, 4737−4742.
(32) Li, J. B.; Bian, H. T.; Chen, H. L.; Wen, X. W.; Hoang, B. T.; Zheng, J. R. *J. Phys. Chem. B* **2013**, *117*, 4274−4283.
(33) Costard, R.; Tyborski, T.; Fingerhut, B. P.; Elsaesser, T. *J. Chem. Phys.* **2015**, *142*, 9.
(34) Costard, R.; Tyborski, T.; Fingerhut, B. P. *Phys. Chem. Chem. Phys.* **2015**, *17*, 29906−29917.
(35) Thogersen, J.; Rehault, J.; Odelius, M.; Ogden, T.; Jena, N. K.; Jensen, S. J. K.; Keiding, S. R.; Helbing, J. *J. Phys. Chem. B* **2013**, *117*, 3376−3388.
(36) Ramasesha, K.; De Marco, L.; Mandal, A.; Tokmakoff, A. *Nat. Chem.* **2013**, *5*, 935−940.
(37) Woutersen, S.; Bakker, H. J. *Nature* **1999**, *402*, 507−509.
(38) Lindner, J.; Vöhringer, P.; Pshenichnikov, M. S.; Cringus, D.; Wiersma, D. A.; Mostovoy, M. *Chem. Phys. Lett.* **2006**, *421*, 329.
(39) Cowan, M. L.; Bruner, B. D.; Huse, N.; Dwyer, J. R.; Chugh, B.; Nibbering, E. T. J.; Elsaesser, T.; Miller, R. J. D. *Nature* **2005**, *434*, 199−202.
(40) Rezus, Y. L. A.; Bakker, H. J. *J. Chem. Phys.* **2005**, *123*, 114502.
(41) Loparo, J.; Fecko, C.; Eaves, J.; Roberts, S.; Tokmakoff, A. *Phys. Rev. B: Condens. Matter Mater. Phys.* **2004**, *70*, 180201.
(42) Loparo, J. J.; Roberts, S. T.; Tokmakoff, A. *J. Chem. Phys.* **2006**, *125*, 13.
(43) Ramasesha, K.; Roberts, S. T.; Nicodemus, R. A.; Mandal, A.; Tokmakoff, A. *J. Chem. Phys.* **2011**, *135*, 054509.
(44) Moilanen, D. E.; Fenn, E. E.; Lin, Y.-S.; Skinner, J. L.; Bagchi, B.; Fayer, M. D. *Proc. Natl. Acad. Sci. U. S. A.* **2008**, *105*, 5295−5300.
(45) Marcus, Y. *J. Solution Chem.* **2009**, *38*, 513−516.
(46) Thamer, M.; De Marco, L.; Ramasesha, K.; Mandal, A.; Tokmakoff, A. *Science* **2015**, *350*, 78−82.
(47) Mandal, A.; Tokmakoff, A. *J. Chem. Phys.* **2015**, *143*, 10.
(48) Ramesh, S. G.; Re, S.; Boisson, J.; Hynes, J. T. *J. Phys. Chem. A* **2010**, *114*, 1255−1269.
(49) Kumar, P. P.; Kalinichev, A. G.; Kirkpatrick, R. J. *J. Phys. Chem. B* **2009**, *113*, 794−802.
(50) Chialvo, A. A.; Vlcek, L. *J. Phys. Chem. B* **2015**, *119*, 519−531.
(51) Baul, U.; Vemparala, S. *Phys. Rev. E* **2015**, *91*, 6.
(52) De Marco, L.; Thämer, M.; Reppert, M.; Tokmakoff, A. *J. Chem. Phys.* **2014**, *141*, 034502.
(53) Fecko, C. J.; Loparo, J. J.; Tokmakoff, A. *Opt. Commun.* **2004**, *241*, 521−528.
(54) Petersen, P. B.; Tokmakoff, A. *Opt. Lett.* **2010**, *35*, 1962−1964.
(55) Helbing, J.; Hamm, P. *J. Opt. Soc. Am. B* **2011**, *28*, 171.
(56) DeFlores, L. P.; Nicodemus, R. A.; Tokmakoff, A. *Opt. Lett.* **2007**, *32*, 2966−2968.
(57) Auer, B. M.; Skinner, J. L. *J. Chem. Phys.* **2008**, *128*, 224511.
(58) Knop, S.; Jansen, T. L. C.; Lindner, J.; Vöhringer, P. *Phys. Chem. Chem. Phys.* **2011**, *13*, 4641−4650.
(59) Paarmann, A.; Hayashi, T.; Mukamel, S.; Miller, R. J. D. *J. Chem. Phys.* **2009**, *130*, 204110.
(60) Ahmed, M.; Namboodiri, V.; Singh, A. K.; Mondal, J. A.; Sarkar, S. K. *J. Phys. Chem. B* **2013**, *117*, 16479−16485.

DOI: 10.1021/jacs.6b05122
J. Am. Chem. Soc. 2016, 138, 9634−9645

(61) Ahmed, M.; Namboodiri, V.; Singh, A. K.; Mondal, J. A. *J. Chem. Phys.* **2014**, *141*, 8.
(62) Huse, N.; Ashihara, S.; Nibbering, E. T. J.; Elsaesser, T. *Chem. Phys. Lett.* **2005**, *404*, 389−393.
(63) Ashihara, S.; Huse, N.; Espagne, a.; Nibbering, E. T. J.; Elsaesser, T. *Chem. Phys. Lett.* **2006**, *424*, 66−70.
(64) Ashihara, S.; Huse, N.; Espagne, A.; Nibbering, E. T. J.; Elsaesser, T. *J. Phys. Chem. A* **2007**, *111*, 743−746.
(65) Imoto, S.; Xantheas, S. S.; Saito, S. *J. Phys. Chem. B* **2015**, *119*, 11068−11078.
(66) Hamm, P.; Stock, G. *Phys. Rev. Lett.* **2012**, *109*, 173201.
(67) Hamm, P.; Stock, G. *Mol. Phys.* **2013**, *111*, 2046−2056.
(68) Robertson, W. H.; Price, E. A.; Weber, J. M.; Shin, J. W.; Weddle, G. H.; Johnson, M. A. *J. Phys. Chem. A* **2003**, *107*, 6527−6532.
(69) Heine, N.; Kratz, E. G.; Bergmann, R.; Schofield, D. P.; Asmis, K. P.; Jordan, K. D.; McCoy, A. B. *J. Phys. Chem. A* **2014**, *118*, 8188−8197.
(70) Hamm, P.; Stock, G. *J. Chem. Phys.* **2015**, *143*, 12.
(71) Waterland, M. R.; Kelley, A. M. *J. Chem. Phys.* **2000**, *113*, 6760−6773.
(72) Moskovits, M.; Michaelian, K. H. *J. Chem. Phys.* **1978**, *69*, 2306−2311.
(73) Mandal, A.; Ramasesha, K.; De Marco, L.; Tokmakoff, A. *J. Chem. Phys.* **2014**, *140*, 204508.

DOI: 10.1021/jacs.6b05122
J. Am. Chem. Soc. 2016, 138, 9634−9645